Supporting Information

Suppression of Dark Current in PbS Quantum Dot Infrared Photodetectors Through the Introduction of a CuInSeS Interfacial Layer

Zuyan Chen[#1,3,4], Tengzuo Huang[#1,2,3,4], Bo Zhang[#1,3,4], Chunyan Wu[1,3,4], Xuanyu Zhang[1,3,4],

Tao Sun[2], Wei Xu[1,3,4], Kai Kang[1,3,4], Chaoyu Xiang*[1,3,4], Ting Zhang*[1,3,4], and Ruifeng Li*[1,3,4]*

[1]Laboratory of Advanced Nano-Optoelectronic Materials and Devices, Qianwan Institute of CNITECH, Ningbo, Zhejiang, 315336, P.R. China.

[2]International Joint Research Center of China for Optoelectronic and Energy Materials, Energy Research Institute, Yunnan University, Kunming, Yunnan 650091, P.R. China.

[3]Laboratory of Advanced Nano-Optoelectronic Materials and Devices, Ningbo Institute of Materials Technology and Engineering, Chinese Academy of Science, Ningbo, Zhejiang, 315201, P.R. China.

[4]Zhejiang Provincial Engineering Research Center of Energy Optoelectronic Materials and Devices, Ningbo Institute of Materials Technology & Engineering, Chinese Academy of Sciences, Ningbo, Zhejiang, 315201, P.R. China.

Materials

Lead(II) acetate trihydrate($Pb(Ac)_2*3H_2O$, 99.998%, Macklin), hexamethyl ldisilathiane (TMS_2, 98%, J&K, China), oleic acid(OA, 90%, Alfa Aesar), octadecene (ODE, 90%, Alfa Aesar), octane(C_8H_{18}, ⩾99%, Aladdin), ethyl acetate ($C_4H_8O_2$, ⩾99.8%, Macklin), ethanol (C_2H_6O, ⩾99.0%, Sigma-Aldrich), zinc acetate dehydrate ($Zn(Ac)_2*2H_2O$, ⩾99.0%, Sigma-Aldrich), tetramethylammonium hydroxide pentahydrate ($(CH_3)_4N(OH)•5H_2O$, ⩾95%, Sigma-Aldrich) dimethyl sulfoxide (DMSO, anhydrous grade, Sigma-Aldrich), ethanol-amine ($HO(CH_2)_2NH_2$, 99.5%, Sigma-Aldrich), 2-Methoxyethanol ($C_3H_8O_2$, 99.5%, Sigma-Aldrich), 1,2-Ethanedithiol ($C_2H_6S_2$, ⩾98%, Alfa Aesar), acetonitrile (ACN, ⩾99.9%, Aladdin), and copper indium selenium sulfur (CuInSeS, purchased from Fullnano Co., Ltd, China) were used as received with no further purification.

Synthesis of Colloidal PbS QDs

This experiment employs the synthetic approach for producing PbS CQDs, following the methodology as described by Wu et al.[1] Initially, a mixture containing 4 mmol of $Pb(Ac)_2•3H_2O$, 3.0 mL of oleic acid, and 20 mL of ODE is introduced into a 50 mL three-necked flask. The solution is stirred at room temperature for 0.5 hours and subsequently degassed at 125 °C for 1 hour. The resultant solution is then heated to 150 °C and maintained at this temperature for 4 hours to yield the Pb precursor. Following this step, the solution is cooled down to 110 °C, and the sulfur (S) source is introduced. For the preparation of the S source, 440 μL of TMS_2 (stored in a nitrogen glovebox) and 3.6 mL of pre-degassed ODE are combined in a 5 mL vial, thoroughly stirred to form the S source. This S source is rapidly injected into the Pb source, and the reaction proceeds for 5 minutes, after which the solution is allowed to naturally cool to room

temperature. Subsequently, 0.5 mL of oleic acid, 5 mL of ethyl acetate, and 15 mL of anhydrous ethanol are added to the solution. The mixture is then subjected to centrifugation at 8000 rpm for 1 minute. Upon removal of the supernatant, 3 mL of n-hexane and 30 mL of anhydrous ethanol are added to the remaining solution, followed by another centrifugation step at 10000 rpm for 3 minutes, repeating this process once. Finally, the resulting precipitate is dissolved in 8 mL of n-octane to obtain the PbS-OA solution.

Synthesis of ZnO nanoparticle

This experiment follows the synthetic method for ZnO as proposed by Qian et al.[2] Zinc acetate and tetramethylammonium hydroxide (TMAH) were used as starting materials, and a solution precipitation method was employed to synthesize zinc oxide nanoparticles. A solution consisting of 25 mL of zinc acetate in dimethyl sulfoxide (DMSO) and a 30 mL solution of TMAH in ethanol were mixed and stirred for 1 hour under ambient conditions. Subsequently, the resulting mixture was washed and dispersed in ethanol at a concentration of 30 mg/mL.

Preparation of NiO_X Precursor

Nickel oxide precursor solution was fabricated by sol-gel method: 24.885 mg of nickel acetate tetrahydrate and 6.1 μL of ethanolamine were dissolved into 1 mL of ethanol, which was stirred at 65 °C for 2 h to form a stable sol-gel.

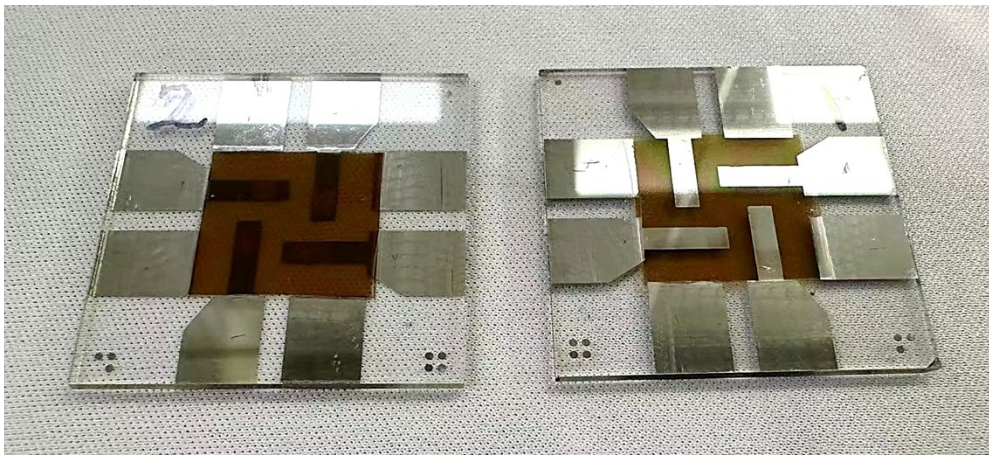

Figure S1. The authentic front and back images of the device.

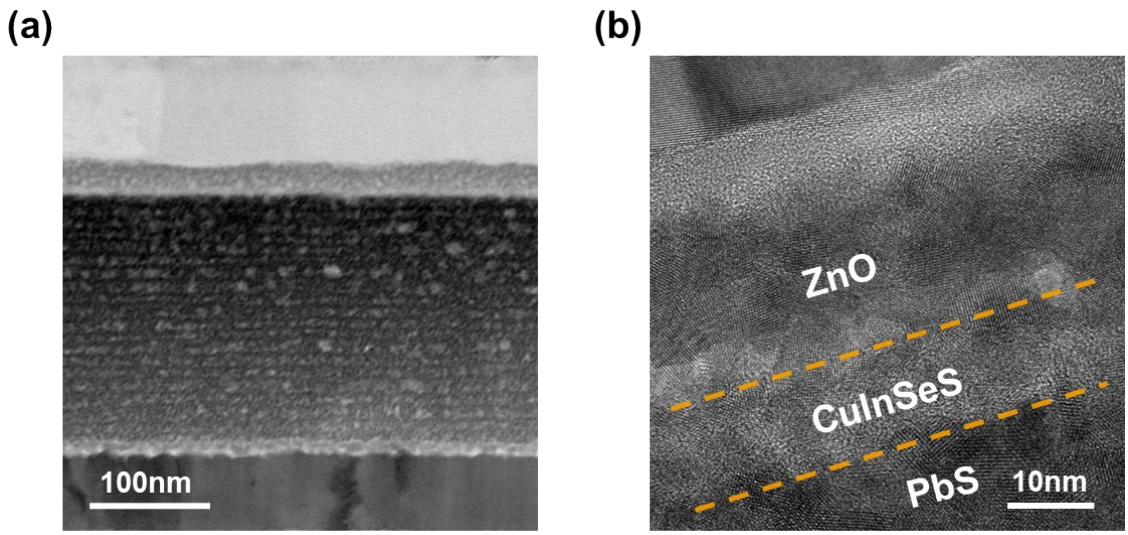

Figure S2. TEM image of the CuInSeS interface layer.

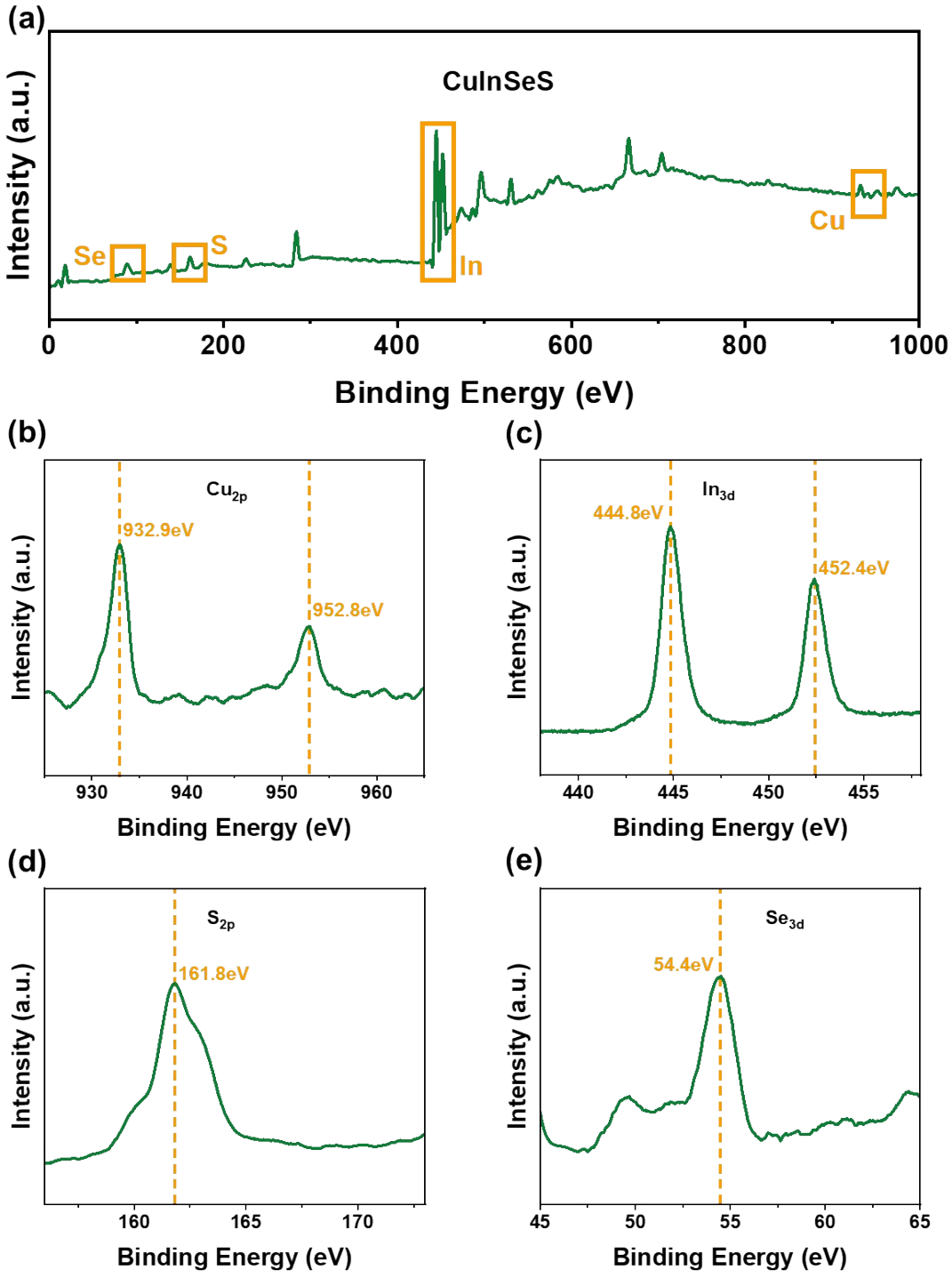

Figure S3. XPS characterization results for CuInSeS. (a) XPS survey spectra of CuInSeS. (b) high-resolution XPS spectra of Cu_{2p}. (c) high-resolution XPS spectra of In_{3d}. (d) high-resolution XPS spectra of S_{2p}. (e) high-resolution XPS spectra of Se_{3d}

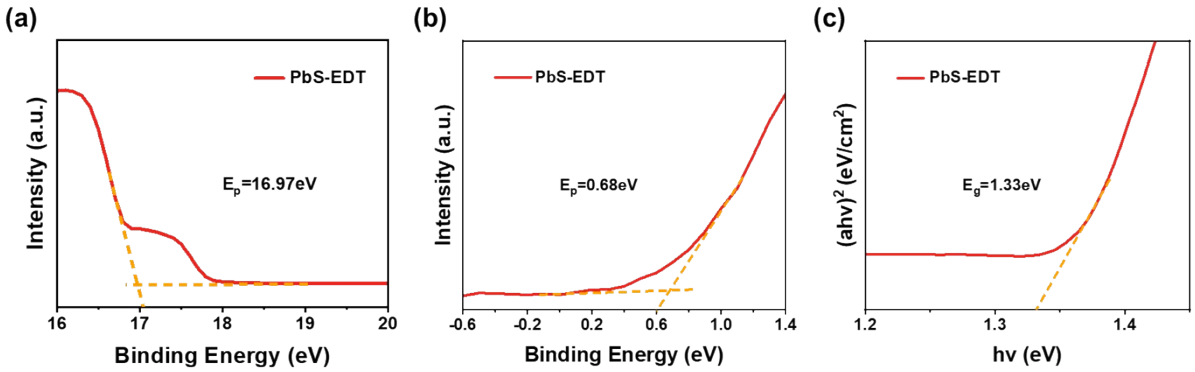

Figure S4. (a) UPS spectra of the secondary electron cutoff region of PbS-EDT and (b) the valence band cutoff region of PbS-EDT. (c) $(ahv)^2$-hv plots of PbS-EDT layer

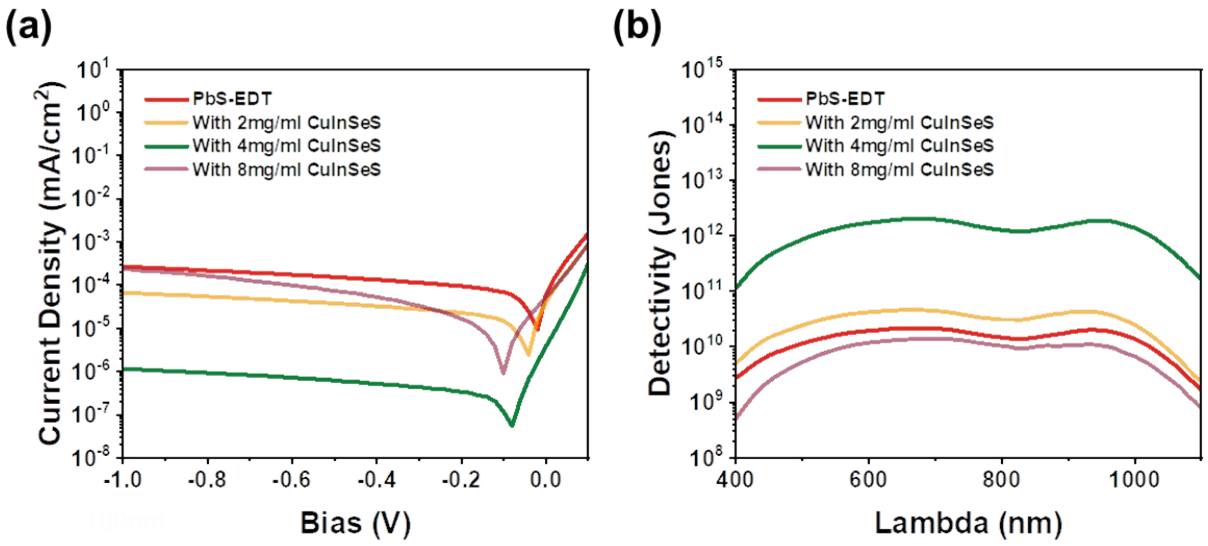

Figure S5. (a) Dark current density versus voltage curves (J_{dark}-V) for PbS-EDT and PbS-EDT/CuInSeS (different concentration) device. (b) Detectivity for the different devices operating at a negative bias of 1V.

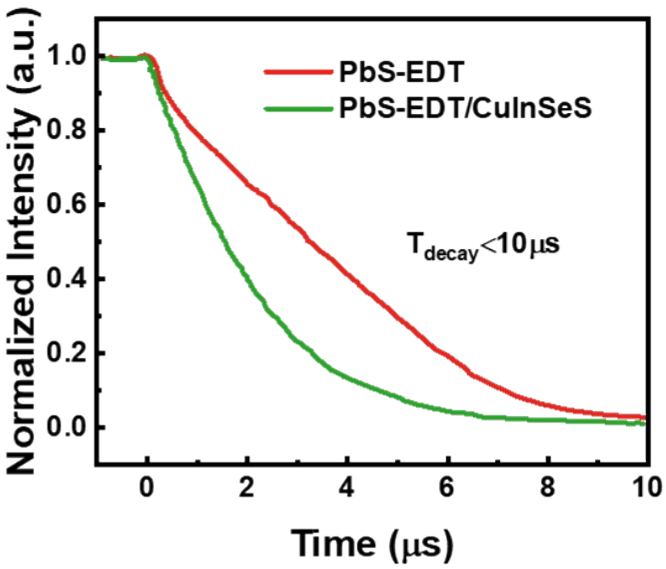

Figure S6. Temporal response comparison of PbS-EDT and PbS-EDT/CuInSeS devices.

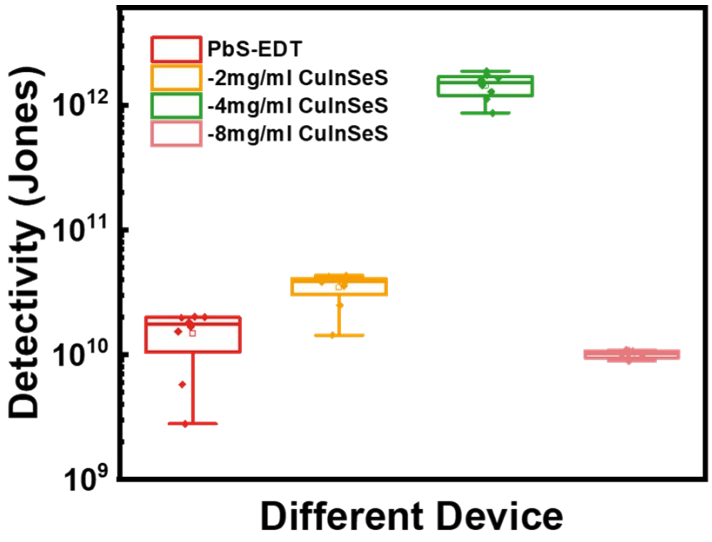

Figure S7. Detectivity of devices with different concentrations of the CuInSeS functional layer. Each dataset comprises data from 8 devices.

Material	Dark current (mA/cm^2)	Response range (nm)	EQE (%)	D*max (Jones)	Ref.
PbS/CuInSeS	**2.19×10^{-7}**	**~940nm**	**29.9%**	**8.57×10^{12}**	**This work**
PbS	**1.32×10^{-4}**	**~1300 nm**	**50.28%**	**2.15×10^{12}**	[3]
PbS	**10^{-4}**	**1350 nm and 930 nm**	**24%**	**2×10^{11}**	[4]
$CuInSe_2$	**10^{-7}**	**370nm**	**-**	**1.6×10^{12}**	[5]
$CuInS_2$	**10^{-5}**	**500~600nm**	**R=0.86A/W**	**3.8×10^{11}**	[6]

Table S1. Comparison table between this work and other similar studies

References:

[1] C. Wu, S. Ding, L. Zhang, F. Huang, G. Qiu, J. Yang, F. Yu, T. Sun, L. Qian, C. Xiang, Enhancing the Absorbance and Carrier Extraction of Lead Sulfide Quantum Dot Solar Cells by the Bilayer ZnO with a Self‐Assembly Optical Structure, Solar RRL, 7 (2023), https://doi.org/10.1002/solr.202300019.
[2] L. Qian, Y. Zheng, J. Xue, P.H. Holloway, Stable and efficient quantum-dot light-emitting diodes based on solution-processed multilayer structures, Nature Photonics, 5 (2011) 543-548, https://doi.org/10.1038/nphoton.2011.171.
[3] S. Lu, P. Liu, J. Yang, S. Liu, Y. Yang, L. Chen, J. Liu, Y. Liu, B. Wang, X. Lan, J. Zhang, L. Gao, J. Tang, High-Performance Colloidal Quantum Dot Photodiodes via Suppressing Interface Defects, ACS Appl Mater Interfaces, 15 (2023) 12061-12069, https://doi.org/10.1021/acsami.2c22774.
[4] O. Atan, J.M. Pina, D.H. Parmar, P. Xia, Y. Zhang, A. Gulsaran, E.D. Jung, D. Choi, M. Imran, M. Yavuz, S. Hoogland, E.H. Sargent, Control over Charge Carrier Mobility in the Hole Transport Layer Enables Fast Colloidal Quantum Dot Infrared Photodetectors, Nano Lett, 23 (2023) 4298-4303, https://doi.org/10.1021/acs.nanolett.3c00491.
[5] R. Guo, T. Shen, J. Tian, Broadband hybrid organic/CuInSe2 quantum dot photodetectors, Journal of Materials Chemistry C, 6 (2018) 2573-2579, https://doi.org/10.1039/c8tc00288f.
[6] Y. Liu, C. Zhao, J. Li, S. Zhao, X. Xu, H.Y. Fu, C. Yu, F. Kang, G. Wei, Highly Sensitive CuInS2/ZnS Core–Shell Quantum Dot Photodetectors, ACS Applied Electronic Materials, 3 (2021) 1236-1243, https://doi.org/10.1021/acsaelm.0c01064.